KERNEL PRINCIPAL COMPONENT ANALYSIS OF THE EAR MORPHOLOGY

Reza Zolfaghari, Nicolas Epain, Craig T. Jin, Joan Glaunès, Anthony Tew

ABSTRACT

This paper describes features in the ear shape that change across a population of ears and explores the corresponding changes in ear acoustics. The statistical analysis conducted over the space of ear shapes uses a kernel principal component analysis (KPCA). Further, it utilizes the framework of large deformation diffeomorphic metric mapping and the vector space that is constructed over the space of *initial momentums*, which describes the diffeomorphic transformations from the reference template ear shape. The population of ear shapes examined by the KPCA are 124 left and right ear shapes from the SYMARE database that were rigidly aligned to the template (population average) ear. In the work presented here we show the morphological variations captured by the first two kernel principal components, and also show the acoustic transfer functions of the ears which are computed using fast multipole boundary element method simulations.

Index Terms— Morphoacoustics, LDDMM, Kernel principal Component Analysis, Ear shape analysis, FM-BEM

1. INTRODUCTION

This paper describes the most important features in the ear shape that change across a population of ears and explores the corresponding changes in ear acoustics. The work forms part of the study of morphoacoustics [1, 2, 3, 4], where the goal is to understand the link between variations in the shape of an ear and their effect on the corresponding set of 3D audio filter functions, referred to as head related impulse responses (HRIRs). HRIRs vary for each listener because each listener has differently shaped ears. There is an HRIR filter for each ear and each direction in space and these HRIR filters enable the rendering of binaural 3D audio for a listener. The purpose of the study is to assist research into the prediction of individualized 3D audio filters for listeners based on the morphology of their ears.

The outer ear is an intricate shape and examining the non-linear variations in the ear morphology between listeners is a challenging task. We consider ear shape diffeomorphisms as belonging to a Riemanian space. In this regard, large deformation diffeomorphic metric mapping (LDDMM) is a framework to perform non-rigid diffeomorphic registration and mapping between images, surfaces, curves and distributions in two and three dimensional space [5, 6, 7, 8, 9, 10]. Diffeomorphic maps provide a smooth, one-to-one transformation between the source and target shape. In particular, considerable work has been undertaken to formulate an algorithm for mapping 3D triangulated surfaces [11, 12].

In a recent paper [13] we show how LDDMM coupled with fast multipole boundary element method (FM-BEM) simulations can assist with the study of morphoacoustics and in [14] we show how a template or population average ear shape can be estimated using LDDMM. Furthermore, in [15] we show how a morphable-model for ear shapes based on the LDDMM framework and the kernel principal component analysis (KPCA) is constructed. The template ear is a critical element of the statistical analysis conducted here, but we leave the description of its calculation to [14, 16] as it is beyond the focus of this paper. While LDDMM permits a multiscale approach to mapping ear shapes as discussed in [14], the statistical analysis of ear shapes presented here is based on single scale LDDMM transformations from the reference template ear to ear shapes that have been aligned to the template ear shape via an affine transformation. In this work we use the LDDMM framework combined with a KPCA technique [16, 17, 18] to perform a statistical analysis of ear morphology. In particular, the statistical analysis conducted here is performed over the linear space of *initial momentums* [19] within the framework of LDDMM. By utilizing a set of coupled differential equations known as the "shooting equations" we examine the morphological variations seen in the ear shape. We use the population of left and right ear shapes in the SYMARE database [20] to conduct a statistical analysis of ear shapes. This paper shows the variations in the ear morphology captured by the first and second kernel principal component and also shows the associated changes in ear acoustics as determined by FM-BEM numerical acoustic simulations.

2. METHODS

2.1. LDDMM Framework

LDDMM [21, 10] is a mathematical framework that can be employed for the registration and morphing of three-dimensional shapes [12, 11]. It is based on theories from functional analysis, variational analysis and reproducible kernel Hilbert spaces. We model a 3D-shape as a mesh with triangular faces, which we refer to as $S(\mathbf{X})$ where $\mathbf{X}$ is the matrix specifying the mesh vertices and S represents the mesh connectivity (the triangular faces). LDDMM models the morphing of $S_1(\mathbf{X})$ to $S_2(\mathbf{Y})$ as a dynamic flow of diffeomorphisms of the ambient space, $\mathbb{R}^3$, in which the surfaces are embedded. This flow of diffeomorphisms, $\phi^{\mathbf{v}}(t,\cdot)$, is defined via the partial differential equation:

$$\frac{\partial \phi^{\mathbf{v}}(t,\mathbf{X})}{\partial t} = \mathbf{v}(t) \circ \phi^{\mathbf{v}}(t,\mathbf{X}) \,, \tag{1}$$

where $\mathbf{v}(t)$ is a time-dependent vector field, $\mathbf{v}(t) : \mathbb{R}^3 \rightarrow \mathbb{R}^3$ for t $\in [0,1]$, which models the infinitesimal efforts of the flow, and $\circ$ denotes function composition. This vector field belongs to a Hilbert space of regular vector fields equipped with a kernel, k_V, and a norm $\| \cdot \|_V$ that models the infinitesimal cost of the flow. In the

R. Zolfaghari and C.T. Jin are with CARLab, School of Electrical and Information Engineering, The University of Sydney, Sydney, Australia. email: reza.zolfaghari@sydney.edu.au,craig.jin@sydney.edu.au.

N. Epain is with IRT b-com, 1219 Avenue Champs Blancs 35510 Cesson-Sévigné , France, email: nicolasepain@free.fr.

A. Tew is with the Department of Electronics, The University of York, Heslington, York, UK. email: tony.tew@york.ac.uk.

J.A. Glaunès is with the MAP5, Université Paris Descartes, Sorbonne Paris Cité 75006 Paris, France. email: alexis.glaunes@mi.parisdescartes.fr.

LDDMM framework, we determine $\mathbf{v}(t)$ by minimizing the cost function, J_{S_1,S_2}:

$$J_{S_1,S_2}\left(\mathbf{v}(t)\right) = \gamma \int_0^1 \|\mathbf{v}(t)\|_V^2 dt + E\left(S_1(\phi^{\mathbf{v}}(1,\mathbf{X})), S_2(\mathbf{Y})\right) , \tag{2}$$

where E is a norm-squared cost measuring the degree of matching between $S_1(\phi^{\mathbf{v}}(1,\mathbf{X}))$ and $S_2(\mathbf{Y})$. In this work we use the Hilbert space of currents [6, 12] to compute E because it is easier and more natural than using landmarks. The parameter γ is a parameter that sets the relative weight of the two terms in the cost function. In this work $\gamma = 5 \times 10^{-5}$.

The optimal $\mathbf{v}(t)$ can be expressed as a sum of momentum vectors, $\boldsymbol{\alpha}_n(t)$, with one momentum vector defined for each of the N vertices in $\mathbf{X}$:

$$\mathbf{v}(t) = \frac{d\mathbf{x}(t)}{dt} = \sum_{n=1}^{N} k_V(\mathbf{x}_n(t), \mathbf{x}(t))\, \boldsymbol{\alpha}_n(t) , \tag{3}$$

where in this work we use the Cauchy kernel defined by:

$$k_V(\mathbf{x},\mathbf{y}) = \frac{1}{1 + \frac{\|\mathbf{x}-\mathbf{y}\|^2}{\sigma_V^2}} , \tag{4}$$

for $\mathbf{x}$ and $\mathbf{y}$ in $\in \mathbb{R}^3$. The σ_V parameter is a scale parameter that determines through the kernel, k_V, the range of influence of the momentum vectors $\boldsymbol{\alpha}_n(t)$. Setting σ_V to a larger value increases the coupling in the motion of vertices that are further apart. In this work, $\sigma_V = 10$ mm.

We now define three fundamental LDDMM operations that are at the core of this work, 1- LDDMM matching, 2- geodesic shooting and 3- diffeomorphic flow. The first LDDMM operation denoted by $\mathscr{M}$ refers to the calculation of the momentum vectors that represent the matching between two shapes S_1 and S_2:

$$\{\boldsymbol{\alpha}_n(t)\}_{1\le n\le N}^{0\le t\le 1} = \mathscr{M}(S_1, S_2) . \tag{5}$$

The second LDDMM operation denoted by $\mathcal{S}$ consists in obtaining the deformed shape $S_2^{'}$ and the time dependent momentum vectors that completely parametrize the deformation between the shapes S_1 to S_2 from the initial momentum vectors:

$$\{S_2^{'}, \{\boldsymbol{\alpha}_n(t)\}_{1\le n\le N}^{0\le t\le 1}\} = \mathscr{S}(S_1, \{\boldsymbol{\alpha}_n(0)\}_{1\le n\le N}) . \tag{6}$$

The operation $\mathcal{S}$ is achieved by solving a set of coupled differential equations know as the *shooting equations* [15]. The third LDDMM operation is known as the diffeomoprhic flow operation $\mathscr{F}$ and uses Eq. 3 and the time dependant momentum vectors $\{\boldsymbol{\alpha}_n(t)\}_{1\le n\le N}^{0\le t\le 1}$ to morph the shape S_1 to shape S_2:

$$S_2^{'} = \mathscr{F}\Big(S_1, \{\boldsymbol{\alpha}_n(t)\}_{1\le n\le N}^{0\le t\le 1}\Big) . \tag{7}$$

In this work, $S_2^{'}$ is very close to S_2 but not identical depending on the LDDMM matching process.

2.2. Kernel Based Principal Component Analysis (KPCA)

The previous section shows how a given shape can be represented as the deformation of another shape through a flow of diffeomorphisms which is completely parameterized using the initial momentum vectors. In this section, we statistically analyse the deformation from the template ear shape, $\overline{E}$, to all ears in the dataset, taking for granted that the template shape has already been computed. We use the kernel principal component analysis (KPCA) to statistically analyse the initial momentum vector data corresponding to the deformations. KPCA uses the same inner product as in the computation of the deformation in the LDDMM cost function. The first step in our analysis is to calculate the momentum vectors for every ear, S_l, in the population of L ears, as follows:

$$\{\boldsymbol{\alpha_n}^{(l)}(t)\} = \mathscr{M}(\overline{E}, S_l) \tag{8}$$

In order to calculate the principal components, we calculate the covariance matrix, $\mathbf{C}$, which expresses the mutual correlation of the different ear shapes in the space of deformations. To compute this matrix we first construct a data matrix $\mathbf{A} \in \mathbb{R}^{3N\times L}$ which contains the initial momentum vectors for the entire population of ears:

$$\mathbf{A} = [\mathbf{a}_1,\ \mathbf{a}_2,\ \ldots,\ \mathbf{a}_L]_{3N\times L} \tag{9}$$

where $\mathbf{a}_l$ denotes the column vector containing all the initial momentum vector coefficients for shape S_l. We then center the data by subtracting the population average momentum vectors. The centred data matrix, $\hat{\mathbf{A}}$, is given by:

$$\hat{\mathbf{A}} = [\hat{\mathbf{a}}_1,\ \hat{\mathbf{a}}_2,\ \ldots,\ \hat{\mathbf{a}}_L]_{3N\times L} \tag{10}$$

where $\hat{\mathbf{a}}_l$ is the vector of the centered momentum vectors for the l-th shape:

$$\hat{\mathbf{a}}_l = \mathbf{a}_l - \bar{\mathbf{a}} \quad \text{with} \quad \bar{\mathbf{a}} = \frac{1}{L}\sum_{i=1}^{L} \mathbf{a}_i . \tag{11}$$

We also form the kernel matrix, $\mathbf{K}$, which contains the values of the kernel function for every pair of vertex positions, $\mathbf{x}_n$, that comprise the vertices, $\mathbf{X}$, of the template shape $\overline{E}$:

$$\mathbf{K} = \begin{bmatrix} \mathbf{K}_{11} & \mathbf{K}_{12} & \ldots & \mathbf{K}_{1N} \\ \mathbf{K}_{21} & \mathbf{K}_{22} & & \vdots \\ \vdots & & \ddots & \vdots \\ \mathbf{K}_{N1} & \ldots & \ldots & \mathbf{K}_{NN} \end{bmatrix} ,$$
$$\mathbf{K}_{mn} = k_V(\mathbf{x}_m, \mathbf{x}_n)\, \mathbf{I}_{3\times 3} , \tag{12}$$

where $\mathbf{I}_{3\times 3}$ denotes the 3×3 identity matrix.

The correlation between two shapes is calculated as the inner product of the initial momentum vectors in the Hilbert space of deformations, V. The correlation between shapes S_i and S_j is given by:

$$c_{ij} = \frac{1}{L-1}\left\langle \{\boldsymbol{\alpha_n}^{(i)}(0)\}, \{\boldsymbol{\alpha_n}^{(j)}(0)\} \right\rangle_V = \frac{1}{L-1}\hat{\mathbf{a}}_i^{\mathsf{T}}\mathbf{K}\,\hat{\mathbf{a}}_j , \tag{13}$$

where $(\cdot)^{\mathsf{T}}$ denotes the transpose of a vector or matrix and $\frac{1}{L-1}$ is a normalization factor. Thus, the covariance matrix for the entire population of ears, $\mathbf{C}$, is given by:

$$\mathbf{C} = \frac{1}{L-1}\hat{\mathbf{A}}^{\mathsf{T}}\mathbf{K}\hat{\mathbf{A}} \tag{14}$$

In order to calculate the principal components, as well as the coordinates of the ears in the basis of the principal components, we perform the singular value decomposition of the covariance matrix $\mathbf{C}$:

$$\mathbf{C} = \mathbf{V}\mathbf{D}\mathbf{V}^{\mathsf{T}} . \tag{15}$$

The matrix of the principal components, $\mathbf{U}$, can be then calculated as:

$$\mathbf{U} = \hat{\mathbf{A}}\mathbf{V}\mathbf{D}^{-\frac{1}{2}} . \tag{16}$$

Note that the principal components are orthogonal in the Hilbert space of deformations, *i.e.*, $\mathbf{U}^\mathsf{T}\mathbf{K}\mathbf{U} = \mathbf{I}$. It follows from Equation (16) that $\hat{\mathbf{A}} = \mathbf{U}\mathbf{D}^{\frac{1}{2}}\mathbf{V}^\mathsf{T}$ and therefore $\mathbf{D}^{\frac{1}{2}}\mathbf{V}^\mathsf{T}$ provides the coordinates of the different ear shapes in the basis of the principal components. Each ear can thus be reconstructed by: (1) computing $\mathbf{a}_l = \bar{\mathbf{a}} + \mathbf{U}\mathbf{D}^{\frac{1}{2}}\mathbf{v}_l$ ($\mathbf{v}_l$ is the l-th column of $\mathbf{V}^\mathsf{T}$); and (2) shooting from the template in the $\mathbf{a}_l$ direction, *i.e.*, $S_l = \mathscr{S}(\overline{E}, \{\mathbf{a}_l\})$.

2.3. Examining the Kernel Principal Components

We now describe how the kernel principal components can be used to examine important changes in the ear morphology and their corresponding acoustics. Each kernel principal component (KPC) captures some form of morphological variation seen in the population of shapes. In mathematical notation the kernel principal components are denoted by $\mathbf{u}_i$, where i signifies the principal component number and also the column i in the matrix $\mathbf{U}$. In order to examine the morphological variations captured by a single principal component, $\mathbf{u}_i$, two steps are involved. In the first step, $\mathbf{u}_i$, is multiplied by a suitable weight factor that is chosen to be a scalar multiple of the eigenvalue, $m\mathbf{D}_{ii}^{\frac{1}{2}}$, for some real value $m \in \mathbb{R}$. Because of the normalization used in Eq. (13), the eigenvalue $\mathbf{D}_{ii}$ is equal to the variance of the scores (coordinates of the ear shapes) belonging to the i^{th} principal component. In the second step, the morphological changes with respect to the template shape can be observed by constructing the ear shape, $E(i, m)$, by using the shooting operation:

$$\{E(i,m), \{\boldsymbol{\alpha}_n(t,i,m)\}\} = \mathscr{S}(\overline{E}, \bar{\mathbf{a}} + m\mathbf{D}_{ii}^{\frac{1}{2}}\mathbf{u}_i) \qquad (17)$$

In order to obtain the acoustic response for the ear shape, the FM-BEM simulations need to be conducted on ears that are attached to the template head and torso shape. However, the template head and torso shape also has the template ear shape, $\overline{E}$, attached. Fig. 1 shows a picture of the template head and torso shape with the template ear attached (i.e $\overline{HTE}$). In order to appropriately morph the template ear shape to the modified ear shape, $E(i, m)$, we use the time-dependent momentum vectors obtained in Eq. 17 to perform a flow operation on the template shape, $\overline{HTE}$, to obtain a template head and torso shape with the modified ear:

$$\overline{HT}E(i,m) = \mathscr{F}(\overline{HTE}, \{\boldsymbol{\alpha}_n(t,i,m)\}) \qquad (18)$$

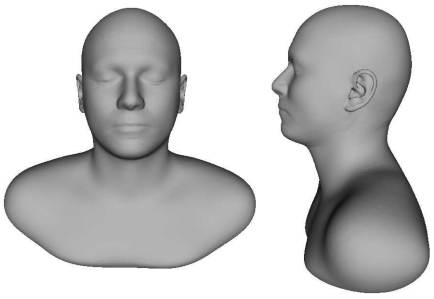

Fig. 1. The template head, torso, and ear shape, $\overline{HTE}$, is shown.

3. EXPERIMENTS

3.1. Experimental setup

We conducted KPCA on ear shapes that were obtained from 62 subjects in the SYMARE database. The right ear shapes of the 62 subjects were reflected to obtain left ear shapes so that we had a total of 124 left ear shapes. In this work, we exclude any scale, rotational or translational variations in ear shapes when conducting the KPCA and thus focus the KPCA solely on structural differences in ear morphology. The structural differences in ear morphology are the most difficult to study. Changes in scale, orientation and position are referred to as affine transformations. Thus, we first optimally align all of the left ear shapes to the template ear, $\overline{E}$, using affine transformations based on a distribution matching technique described in [5].

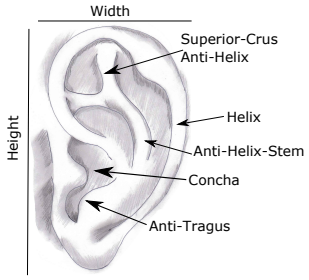

Fig. 2. The structure and anatomical names for parts of the external ear are shown. Adopted from [22].

In order to observe structural differences in ear shape, KPCA was performed on the 124 left ear shapes that were aligned to the template ear via an affine transformation. The KPCA was performed as detailed in Section 2.2. New ear shapes were generated by varying the weights corresponding to the first and second kernel principal components as described in the previous section. More precisely, new ear shapes were obtained using Eq. 17 for values of $m \in B_1 = \{\pm 7, \pm 2, \pm 1, 0\}$. In order to study the acoustics of the new ear shapes, the template, $\overline{HTE}$, was modified according to Eq. 18 to obtain $\overline{HT}E(i,m)$ for $m \in B_2 = \{\pm 2, \pm 1, 0\}$ and $i \in \{1, 2\}$. The only reason for generating ear morphologies at the large and nonsensical values of $m = \pm 7$ was to clearly visualize how the changes in the kernel principal component weights relate to changes in the ear morphology.

HRIRs corresponding to the shapes $\overline{HT}E(i,m)$ were generated using FM-BEM simulations. For this work the Coustyx software by Ansol was used [23]. The simulations were performed by the FM-BEM solver using the Burton-Miller Boundary Integral Equations (BIE) and the Galerkin implementaion. Using the acoustic reciprocity principal, a single simulation is used to determine all of the HRIRs in one go by placing a source on a surface mesh element that forms part of the blocked ear canal and then setting a uniform normal velocity boundary condition on this surface element. A post-processing step was used to refine the meshes prior to the FM-BEM simulation using the open-source software ACVD [24]. The meshes had a critical frequency of 26 kHz for six elements per acoustic wavelength and further, met the FM-BEM mesh criterion detailed in [20, 25].

3.2. Results

Fig. 3 shows the ear shapes that have been generated from the template ear by changing the weights corresponding to the first and second principal components. The differences with respect to the template ear are highlighted in color using a normalized dissimilarity measure based on currents [15]. By changing the weights corresponding to the first and second kernel principal components, there are changes to the size and structure of features in the pinna. Please keep in mind that the overall size and rotation of the ears in the dataset have been aligned to the template, so that it is the structural features of the pinna

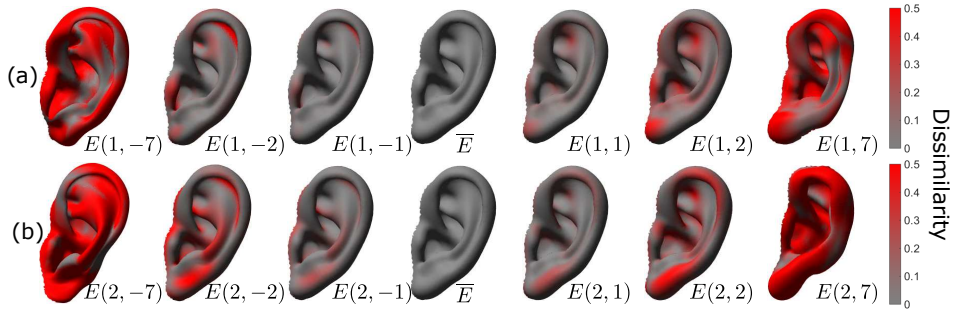

Fig. 3. Ear morphologies are shown corresponding to systematic changes in (a) the first and (b) the second kernel principal components. Note that $E(i,m)$ denotes the template ear, $\overline{E}$, modified with the i-th KPC using a weight of m standard deviations. The degree of difference between the given ear shape and the template ear shape are highlighted in color using a normalized dissimilarity measure based on currents [15]. (The colors have constant luminance and so do not appear in grey-scale, instead please view the online version.)

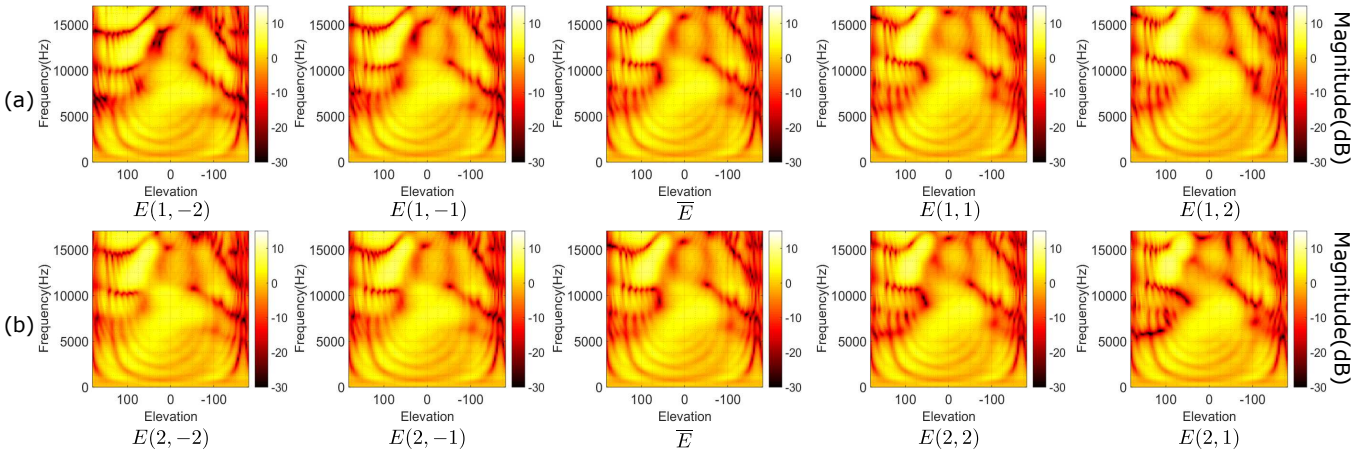

Fig. 4. DTFs on the median plane are shown for some of the ear shapes in Fig. 3. The elevation angles are in degrees with positive angles corresponding to the front and negative angles corresponding to the back. Note that 0° corresponds to straight up and 180° and -180° correspond to straight down.

that are changing. For the ensuing discussion, please refer to both Fig. 3 and Fig. 2 which shows the names of anatomical features of the outer ear. For the first KPC, when $m = -7$ the ear appears to be wider in width and have a larger Concha and Superior-Crus-Anti-Helix region. On the other hand, when $m = 7$ the ear appears to fold inwards and become narrower. For the second KPC, when $m = -7$ the Anti-Helix-Stem has moved outwards (even out of the ear) and the Superior-Crus-Anti-Helix region is larger. On the other hand, when $m = 7$ the opening of the Concha is very wide, making the Superior-Crus-Anti-Helix region smaller and pushing down the Anti-Tragus.

Consider now the acoustics of the ears. Fig. 4 shows the log-magnitude of the Directional Transfer Functions (DTFs) [26] in the median plane for several of the ear shapes in Fig. 3. In order to quantitatively evaluate the differences in the median plane DTFs, we used a measure similar to that described in [26]. Assume the log-magnitude spectra are given for two DTFs, so that we have $D_1(f)$ and $D_2(f)$. We then compute a log-magnitude spectral difference, σ, as:

$$\sigma = \sqrt{\frac{1}{N}\sum_{n=1}^{N}\left[\left(D_1(f_n) - \overline{D}_1\right) - \left(D_2(f_n) - \overline{D}_2\right)\right]^2}, \quad (19)$$

where N is the number of frequency bins and $\overline{D}$ is the mean value of $D(f)$. The log-magnitude spectral difference between the median plane DTFs for $E(i,m)$ and $\overline{E}$ were computed and then averaged across all elevations on the median plane (see Table 1). The average log-magnitude spectral difference for both KPCs is fairly similar and varies between 3 and 5.3 dB.

m	-2	-1	1	2
$i=1$	5.3	4.0	3.1	4.2
$i=2$	4.4	3.3	3.3	4.7

Table 1. The average log-magnitude spectral difference for the median plane DTFs are shown in dB for the first and second KPC.

4. CONCLUSION

This paper shows variations in ear morphology that commonly occur across a population of ears and the associated changes in the ear acoustics. The analysis was performed using KPCA within the LDDMM framework. The morphological and corresponding acoustic variations of the ear shapes within the SYMARE population are shown for the first and second kernel principal components. The work detailed in this paper forms part of ongoing morphoacoustics research. Future studies will further examine the relationship between the kernel principal components for ear shape and the associated changes in ear acoustics.

5. REFERENCES

[1] A. Tew, C. Hetherington, and J. Thorpe, "Morphoacoustic perturbation analysis," in *Proceedings of the Joint meeting of the 11th Congrès Français d'Acoustique and the 2012 Annual Meeting of the Institute of Acoustics from UK*, Nantes, France, 2012, pp. 867–872.

[2] D. Y. N. Zotkin, J. Hwang, R. Duraiswaini, and L. S. Davis, "Hrtf personalization using anthropometric measurements," in *Applications of Signal Processing to Audio and Acoustics, 2003 IEEE Workshop on.* Ieee, 2003, pp. 157–160.

[3] C. Jin, P. Leong, J. Leung, A. Corderoy, and S. Carlile, "Enabling individualized virtual auditory space using morphological measurements," in *Proceedings of the First IEEE Pacific-Rim Conference on Multimedia (2000 International Symposium on Multimedia Information Processing)*. Citeseer, 2000, pp. 235–238.

[4] P. Mokhtari, H. Takemoto, R. Nishimura, and H. Kato, "Pinna sensitivity patterns reveal reflecting and diffracting surfaces that generate the first spectral notch in the front median plane," in *Acoustics, Speech and Signal Processing (ICASSP), 2011 IEEE International Conference on*. IEEE, 2011, pp. 2408–2411.

[5] J. Glaunes, A. Trouve, and L. Younes, "Diffeomorphic matching of distributions: a new approach for unlabelled point-sets and sub-manifolds matching," in *Computer Vision and Pattern Recognition, 2004. CVPR 2004. Proceedings of the 2004 IEEE Computer Society Conference on*, vol. 2, June 2004, pp. II–712–II–718 Vol.2.

[6] J. Glaunés, A. Qiu, M. I. Miller, and L. Younes, "Large deformation diffeomorphic metric curve mapping," *International Journal of Computer Vision*, vol. 80, pp. 317–336, 2008.

[7] M. F. Beg, M. I. Miller, A. Trouvé, and L. Younes, "Computing large deformation metric mappings via geodesic flows of diffeomorphisms," *International Journal of Computer Vision*, vol. 61, no. 2, pp. 139–157, 2005.

[8] P. Dupuis, U. Grenander, and M. Miller, "Variational problems on flows of diffeomorphisms for image matching," *Quarterly of applied mathematics*, vol. 56, no. 3, p. 587, 1998.

[9] M. Miller, A. Trouvé, and L. Younes, "On the metrics and euler-lagrange equations of computational anatomy," *Annual review of biomedical engineering*, vol. 4, no. 1, pp. 375–405, 2002.

[10] M. Miller and L. Younes, "Group actions, homeomorphisms, and matching: A general framework," *International Journal of Computer Vision*, vol. 41, no. 1, pp. 61–84, 2001.

[11] M. Vaillant, A. Qiu, J. A. Glaunés, and M. I. Miller, "Diffeomorphic metric surface mapping in subregion of the superior temporal gyrus," *NeuroImage*, vol. 34, no. 3, pp. 1149 – 1159, 2007.

[12] M. Vaillant and J. A. Glaunés, "Surface matching via currents," in *Information Processing in Medical Imaging*, ser. Lecture Notes in Computer Science, G. E. Christensen and M. Sonka, Eds. Springer Berlin Heidelberg, 2005, vol. 3565, pp. 381–392.

[13] R. Zolfaghari, N. Epain, C. T. Jin, J. Glaunes, and A. Tew, "Large deformation diffeomorphic metric mapping and fast-multipole boundary element method provide new insights for binaural acoustics," in *Acoustics, Speech and Signal Processing (ICASSP), 2014 IEEE International Conference on*, May 2014, pp. 2863–2867.

[14] R. Zolfaghari, N. Epain, C. Jin, A. Tew, and J. Glaunes, "A multiscale lddmm template algorithm for studying ear shape variations," in *Signal Processing and Communication Systems (ICSPCS), 2014 8th International Conference on*, Dec 2014, pp. 1–6.

[15] R. Zolfaghari, N. Epain, C. T. Jin, J. Glauns, and A. Tew, "Generating a morphable model of ears," in *2016 IEEE International Conference on Acoustics, Speech and Signal Processing (ICASSP)*, March 2016, pp. 1771–1775.

[16] M. Vaillant, M. Miller, L. Younes, A. Trouvé *et al.*, "Statistics on diffeomorphisms via tangent space representations," *NeuroImage*, vol. 23, no. 1, p. 161, 2004.

[17] C. Cury, J. Glaunès, M. Chupin, and O. Colliot, "Analysis of anatomical variability using diffeomorphic iterative centroid in patients with alzheimer's disease," *Computer Methods in Biomechanics and Biomedical Engineering: Imaging & Visualization*, no. ahead-of-print, pp. 1–9, 2015.

[18] C. Cury, "Statistical shape analysis of the anatomical variability of the human hippocampus in large populations." Ph.D. dissertation, Université Pierre et Marie Curie-Paris VI, 2015.

[19] M. Miller, A. Trouv, and L. Younes, "Geodesic shooting for computational anatomy," *Journal of Mathematical Imaging and Vision*, vol. 24, no. 2, pp. 209–228, 2006. [Online]. Available: http://dx.doi.org/10.1007/s10851-005-3624-0

[20] C. Jin, P. Guillon, N. Epain, R. Zolfaghari, A. van Schaik, A. Tew, C. Hetherington, and J. Thorpe, "Creating the sydney york morphological and acoustic recordings of ears database," *Multimedia, IEEE Transactions on*, vol. 16, no. 1, pp. 37–46, Jan 2014.

[21] U. Grenander and M. I. Miller, "Computational anatomy: An emerging discipline," *Quarterly of applied mathematics*, vol. 56, no. 4, pp. 617–694, 1998.

[22] "External ear anatomy," http://clinanat.com/, Clinical Anatomy Associates, Inc.

[23] "Coustyx," http://ansol.us/Products/Coustyx/, Ansol.

[24] "Acvd," http://www.creatis.insa-lyon.fr/site/en/acvd, CREATIS Medical Imaging Research Center.

[25] N. A. Gumerov, A. E. O'Donovan, R. Duraiswami, and D. N. Zotkin, "Computation of the head-related transfer function via the fast multipole accelerated boundary element method and its spherical harmonic representation," *The Journal of the Acoustical Society of America*, vol. 127, no. 1, 2010.

[26] J. C. Middlebrooks, "Individual differences in external-ear transfer functions reduced by scaling in frequency," *The Journal of the Acoustical Society of America*, vol. 106, no. 3, pp. 1480–1492, 1999.